Sensing and Bio-Sensing Research 48 (2025) 100799

Contents lists available at ScienceDirect

Sensing and Bio-Sensing Research

journal homepage: www.elsevier.com/locate/sbsr

Colorimetric sensing of Au^{3+} ions in aqueous media: A xanthene-based probe for rapid and visual detection

Nuriye Tuna Subasi *

Department of Food Engineering, Faculty of Engineering and Architecture Kırşehir Ahi Evran University, Kırşehir 40100, Turkey

ARTICLE INFO

Keywords:
Au^{3+}
Colorimetric sensor
Xanthene
Rapid naked eye detection

ABSTRACT

Ionic gold species play a pivotal role in various chemical and biological systems due to their unique properties. However, even trace amounts of Au^{3+} ions (as low as 200 μM) can pose significant toxicity risks to living organisms, underscoring the need for accurate and rapid detection methods. In this study, we present the design and characterization of a novel colorimetric sensor, TS-Xan, specifically developed for Au^{3+} ion detection. TS-Xan, a xanthene-derived probe, functions as a reversible sensor. Its molecular structure was characterized using nuclear magnetic resonance (NMR) spectroscopy and high-resolution mass spectrometry (HRMS). The sensor exhibited excellent sensitivity toward Au^{3+} ions, inducing a distinct colorimetric shift from yellow to violet, visible to the naked eye in aqueous media. UV–vis absorption studies revealed the formation of a new absorption band at 570 nm, corresponding to the TS-Xan-Au^{3+} complex. HRMS analysis further elucidated the binding stoichiometry, confirming a 2:1 (TS-Xan:Au^{3+}) complex formation. To enhance its practical applicability, TS-Xan-coated test strips were fabricated, demonstrating exceptional sensitivity and reliability for on-site Au^{3+} detection. This work introduces a promising and user-friendly approach for gold ion sensing, with potential applications in environmental monitoring, industrial waste analysis and bioanalytical fields.

1. Introduction

Gold (Au), a chemically inert metal, has been highly valued throughout human history and extensively utilized in artworks, jewelry, and decorative objects. In recent years, gold and its various forms—including gold nanoparticles (AuNPs), gold complexes, and ionic gold species—have gained significant attention due to their unique physicochemical properties, leading to broad applications in chemical and biological fields. Gold nanoparticles (AuNPs) have been widely employed in drug delivery, bioimaging, and as functional additives in cosmetic products [1–4]. Beyond nanoparticles, ionic gold species, particularly Au(I) and Au(III), are well known for their ability to selectively activate alkyne π-bonds, making them valuable catalysts in synthetic organic chemistry [5–11]. These gold-catalyzed transformations often proceed under mild conditions, typically at room temperature within minutes, highlighting Au ions as one of the most efficient catalytic systems available today. Additionally, metallic gold, due to its exceptional biocompatibility and anticancer properties, has fueled growing interest in biomedical and environmental research. Gold-based pharmaceuticals are currently employed in the treatment of various diseases, including cancer, asthma, and HIV [12–15]. Moreover, gold compounds exhibit anti-inflammatory properties, making them effective therapeutic agents for rheumatoid arthritis and tuberculosis [16,17]. Despite these remarkable advantages, Au(III) ions pose significant biological risks. They exhibit a strong affinity for DNA and enzymes, leading to cytotoxic effects that can cause kidney, liver, and peripheral nervous system damage [18–21]. Studies have reported that exposure to even 200 μM $AuCl_3$ can induce severe toxicity and organ damage [22]. Although Au^{3+} ions are not naturally present in biological systems, exposure can occur through various external sources such as the use of gold-based therapeutic agents (e.g., anti-arthritic drugs), diagnostic gold nanoparticles, or environmental contamination. Accumulation of Au^{3+} ions in biological tissues can lead to cytotoxicity, oxidative stress, and disruption of normal cellular functions. Therefore, monitoring the presence of Au^{3+} ions in biological and environmental samples is crucial for health and safety considerations. Given these concerns, the development of rapid, selective, and effective detection methods for Au(III) ions is critical, particularly for monitoring their presence in environmental samples, agrochemicals, and biological systems.

Classical analytical techniques such as atomic absorption

* Corresponding author.
E-mail address: nsubasi@ahievran.edu.tr.

https://doi.org/10.1016/j.sbsr.2025.100799
Received 3 March 2025; Received in revised form 20 April 2025; Accepted 28 April 2025
Available online 29 April 2025

spectroscopy (AAS) [23,24], inductively coupled plasma mass spectrometry (ICP-MS) [25,26], flame atomic absorption spectrometry (FAAS) [27,28], and electrochemical analysis [29,30] are widely employed for the detection of various gold species. Although these methods offer high selectivity and sensitivity, they suffer from several drawbacks, including the requirement for expensive instrumentation, labor-intensive multi-step sample preparation, and prolonged analysis times. Furthermore, these techniques necessitate highly skilled personnel, limiting their accessibility for routine and on-site analysis [31]. To address these challenges, fluorescence spectroscopy has emerged as a promising alternative, offering high sensitivity, selectivity, cost-effectiveness, and ease of operation. Fluorescent probes have gained significant attention for the detection of Au^{3+} ions in chemical and biological systems due to their rapid response and straightforward application [32–36]. Given the well-known alkynophilicity of gold ions, numerous molecular sensors have been developed by modifying fluorophore molecules with alkyne-functionalized groups, leveraging their unique photophysical properties for enhanced Au^{3+} detection [37–42].

To this end, various molecular sensors, including colorimetric and fluorescent probes, have been developed and extensively studied for the detection of Au^{3+} ions. These sensors are designed based on specialized fluorophores such as fluorescein [43–46], BODIPY [37,47–51], coumarin [40,52,53], rhodamine [54–57], naphthalimide [58,59], quinoline [60], and poly(phenyldiethylene) [61], all of which have demonstrated promising analytical performance. However, the sensing mechanism of these probes typically relies on an irreversible chemical reaction, which results in the structural modification of the probe molecules. Consequently, these sensors are consumed during the detection process and cannot be reused. Moreover, many of these probes suffer from poor selectivity, as their detection mechanisms are often susceptible to interference from other alkynophilic metal ions such as Au^{+}, Ag^{+}, Pd^{2+}, Ni^{2+}, Cu^{2+}, and Hg^{2+}. Therefore, there is a critical need to develop novel sensing strategies for Au^{3+} detection that are not only highly selective and reusable but also free from cross-reactivity with other alkynophilic metal species.

In recent years, colorimetric detection methods have garnered significant attention across various scientific fields due to their numerous advantages. One of their most compelling features is their rapid response and operational simplicity, allowing for instant visual observation and in situ detection without the need for sophisticated instrumentation. A major advantage of colorimetric techniques is their accessibility, as they facilitate the direct, naked-eye detection of target analytes, thereby eliminating the reliance on complex analytical tools. This inherent simplicity not only enhances user-friendliness but also provides exceptional portability, making colorimetric sensors ideal for on-the-spot analysis—even in resource-limited settings or by individuals without specialized training [62].

In this study, we introduce a novel xanthene-based colorimetric probe (TS-Xan) developed for the rapid, sensitive, and selective detection of Au^{3+} ions in aqueous environments via naked-eye observation. As illustrated in Fig. 1, TS-Xan is strategically designed by incorporating a 2-hydrazinopyridine (2-HP) functional group into the xanthene (Xan) framework. The 2-HP moiety, known for its strong binding affinity toward Au^{3+} ions, plays a crucial role in the probe's sensing mechanism. This design enables efficient and highly selective interaction between the 2-HP group and Au^{3+} ions, facilitating a rapid and distinct colorimetric response. The utilization of 2-HP as a metal receptor has been well-documented in the literature [63], further supporting its applicability in selective metal ion detection.

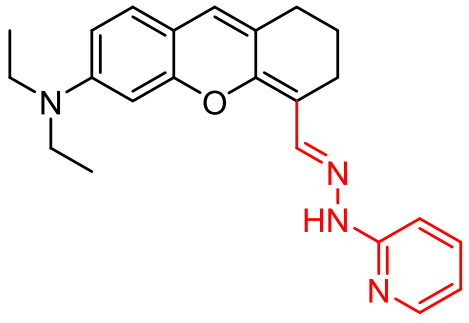

Fig. 1. Structure of the probe (TS-Xan).

Upon exposure to Au^{3+} ions, TS-Xan undergoes an instantaneous colorimetric shift from yellow to violet in aqueous solution, enabling direct naked-eye detection without the need for a spectrometric device. The selectivity and sensitivity of TS-Xan toward Au^{3+} detection were systematically evaluated through UV–vis absorption studies. Furthermore, to assess the practical applicability of the probe, TS-Xan-coated test strips were prepared and exposed to Au^{3+} ions in phosphate-buffered saline (PBS). The observed color change demonstrated the sensor's potential for on-site Au^{3+} detection, further highlighting its suitability for real-world applications

2. Experimental

2.1. General methods

All reactions were carried out in oven-dried glassware under an argon atmosphere unless otherwise stated. All reagents were obtained from commercial suppliers (Sigma-Aldrich, Merck) and used without further purification. Thin-layer chromatography (TLC) was performed on pre-coated silica gel $60F_{254}$ aluminum plates (Merck), and spots were visualized under UV light ($\lambda = 254$ nm). Column chromatography was conducted using silica gel 60 (40–63 μm). Nuclear magnetic resonance (NMR) spectra were recorded in chloroform-*d* on a Varian VNMRJ 400 and Bruker Avance 400 spectrometer (400 MHz). Chemical shifts (δ) are reported in parts per million (ppm) relative to internal standards: $CHCl_3$ (^{1}H: δ= 7.27 ppm), $CDCl_3$ (^{13}C: δ = 77.0 ppm) and d_6-DMSO (^{1}H: δ = 2.50 ppm), d_6-DMSO (^{13}C: δ = 39.52 ppm). UV–vis absorption spectra were obtained using a Shimadzu UV-2550 spectrophotometer. pH measurements were performed with a Hanna HI-8014 pH meter. All measurements were conducted in triplicate for accuracy. High-resolution mass spectrometry (HRMS) analyses were performed using a Bruker apex IV FTMS spectrometer, and mass-to-charge (*m/z*) ratios are reported in atomic mass units (amu).

Synthesis of the probe molecule: The synthesis of the TS-Xan probe was carried out via a three-step synthetic process starting from cyclohexanone, following the synthetic route outlined in scheme 1 in accordance with previously reported literature procedures [63–65].

2.2. Synthesis of compound 2 (2-bromocyclohex-1-ene-1-carbaldehyde)

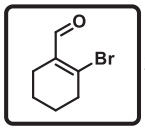

2,4 mL dry DMF and 8 mL $CHCl_3$ were placed in a 100 mL round-bottom flask and cooled to 0 °C with an ice bath. To this solution, phosphorus tribromide (PBr_3, 2.31 mL) was then added dropwise over 10 min, and the reaction mixture was stirred at room temperature for 45 min. Subsequently, cyclohexanone (1.0 mL) dissolved in 3 mL $CHCl_3$ was added, and the reaction was allowed to proceed overnight at room temperature. Upon completion, the reaction mixture was poured into ice water, followed by the slow addition of $NaHCO_3$ until the pH reached approximately 7. The layers were separated, and the aqueous phase was extracted three times with $CHCl_3$. The combined organic layers were dried over anhydrous Na_2SO_4, and the solvent was removed under reduced pressure. The crude product was then purified by flash column chromatography (1:7, ethyl acetate/hexane). ^{1}H NMR (400 MHz, $CDCl_3$) *δ*: 10.12 (s, 1H), 2.64 (t, 2H), 2.28 (t, 2H), 1.86 (t,

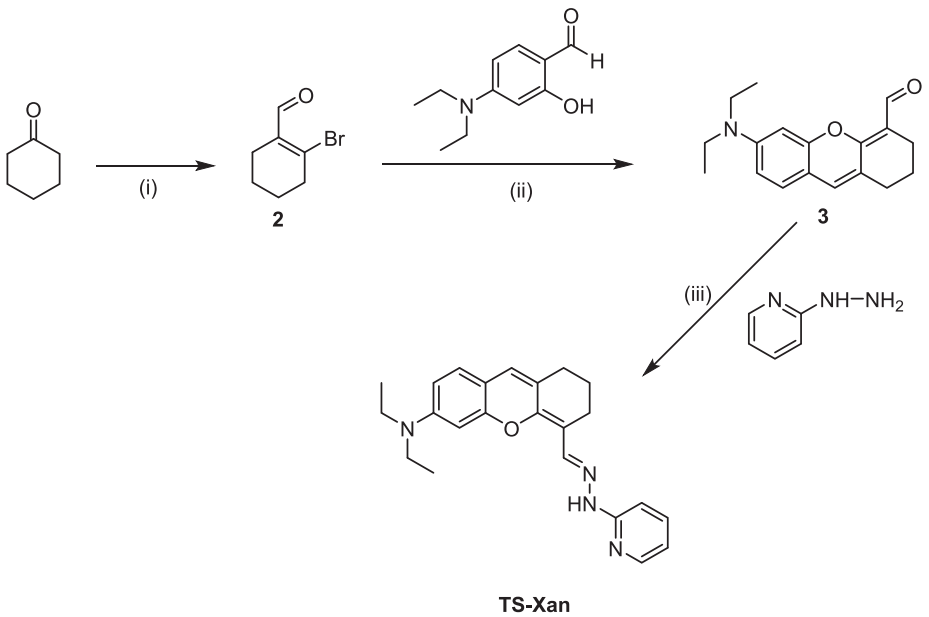

Scheme 1. Synthetic route of TS-Xan. (i) PBr_3, DMF, $CHCl_3$, overnight, RT (ii) Cs_2CO_3, DMF, 3 h, RT (iii) ethanol, glacial acetic acid, reflux, 2 h

4H). ^{13}C NMR (100 MHz, $CDCl_3$) δ: 193.9, 144.7, 140.4, 37.9, 24.1, 22.4, 21.8

2.3. Synthesis of compound 3 (6-(diethylamino)-2,3-dihydro-1H-xanthene-4-carbaldehyde)

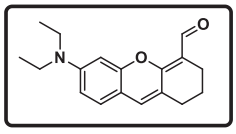

4-(Diethylamino) salicylaldehyde (200 mg, 1.035 mmol) and Cs_2CO_3 (1 g, 3.105 mmol) were dissolved in 3 mL dry DMF in a 50 mL round-bottom flask. In a separate vial, compound 2 (400 mg, 2.07 mmol) was dissolved in 1 mL of dry DMF and then injected into the reaction flask. The reaction mixture was stirred at room temperature for 3 h. upon completion, the reaction mixture was washed with brine and extracted three times with dichloromethane (DCM). The combined organic layers were dried over anhydrous Na_2SO_4, and the solvent was removed under reduced pressure. The crude product was then purified by flash column chromatography (1:2, ethyl acetate/hexane). ^{1}H NMR (400 MHz, $CDCl_3$) δ 10.28 (s, 1H), 7.01 (d, J = 8.6 Hz, 1H), 6.64 (s, 1H), 6.27 (s, 1H), 6.37 (s, 1H), 3.38 (t, J = 7.1 Hz, 4H), 2.56 (m, 2H), 2.46 (t, J = 6.1 Hz, 2H), 1.68 (m, 2H), 1.19 (t, J = 7.1 Hz, 6H). ^{13}C NMR (100 MHz, $CDCl_3$) δ 192.8, 169.3, 155.6, 150.1, 140.6, 105,8, 105.2, 129.9, 122.4, 119,6, 93.5, 47.4, 30.2, 29.6, 18.5, 122.8

2.4. Synthesis of compound TS-Xan [(E)-N,N-diethyl-4-((2-(pyridin-2-yl)hydrazineylidene)methyl)-2,3-dihydro-1H-xanthen-6-amine]

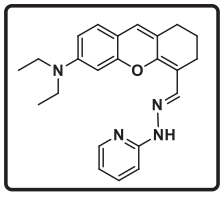

Compound 3 (45 mg, 0.16 mmol) and 2-hydrazinopyridine (20 mg, 0.18 mmol) were dissolved in 5 mL ethanol in a 50 mL round-bottom flask. Subsequently, 1–2 drops of glacial acetic acid were added, and the reaction mixture was refluxed for 2 h. the progress of the reaction was monitored by thin-layer chromatography (TLC). Upon completion, the reaction mixture was cooled to room temperature, and the solvent was removed under reduced pressure. The resulting crude product was purified by silica gel column chromatography (1:5, ethyl acetate/hexane) to afford the probe molecule (TS-Xan) as a yellow oil (37.2 mg, 62 % yield). ^{1}H NMR (400 MHz, d_6-DMSO) δ 10.51 (s, 1H), 8.38 (s, 1H), 8.05 (s, 1H), 7.56–7.51 (m, 1H), 7.08–6.87 (m, 2H), 6.71–6.57 (m, 1H), 6.38–6.27 (m, 2H), 6.14 (s, 1H), 2.48 (m, 8H), 1.63–1.57 (m, 2H), 1.27–0.98 (m, 6H). ^{13}C NMR (100 MHz, d_6-DMSO) δ 157.62, 154.24, 149.21, 148.74, 148.20, 138.07, 137.60 (s), 127.41 (s), 124.71 (s), 121.16 (s), 114.52 (s), 110.45 (s), 108.32 (s), 106.73 (s), 106.41 (s), 96.98 (s), 44.31 (s), 29.67 (s), 23.71 (s), 21.19 (s), 12.97 (s). HRMS (ESI), m/z calcd for $C_{46}H_{52}AuClN_8O_2$ [2TS-Xan + Au^{3+}+Cl], 980.36 found 980.50

3. Results and discussion

A novel xanthene-based colorimetric sensor, incorporating 2-hydrazinopyridine (2-HP) as the metal-binding receptor, was carefully designed for Au^{3+} ion detection. The synthesis of the TS-Xan probe was accomplished through a three-step synthetic route, starting from cyclohexanone, as depicted in scheme 1 and following established literature procedures [64–66]. In the first step, cyclohexanone was reacted with phosphorus tribromide (PBr_3) and *N,N*-dimethylformamide (DMF) in chloroform ($CHCl_3$) to yield compound 1. Subsequently, compound 2 was obtained by reacting compound 1 with 4-(diethylamino)salicylaldehyde, leading to the formation of the xanthene derivative. In the final step, TS-Xan was synthesized via a condensation reaction between the xanthene derivative and 2-HP, yielding the target probe with a 62 % efficiency. The structural characterization of TS-Xan was confirmed using nuclear magnetic resonance (NMR) spectroscopy and high-resolution mass spectrometry (HRMS). Detailed spectral data and analytical results can be found in the supporting information

For the colorimetric evaluation of the synthesized probe, Au^{3+} ions (10 μM, 1 eq.) were added to a TS-Xan solution (10 μM) in phosphate-buffered saline (PBS, 10 mM, pH 7.4, 25 °C), and the resulting changes were recorded using UV–vis absorption spectroscopy. Prior to the addition of Au^{3+} ions, the UV–vis spectrum exhibited two distinct absorption bands at 320 nm and 441 nm. Upon the introduction of Au^{3+} ions, a rapid and visually perceptible color change from yellow to violet was observed in the solution. Simultaneously, in the UV–vis spectrum, the absorption band at 441 nm disappeared, and a new peak emerged at 570 nm, as depicted in Fig. 2. This distinct colorimetric transition and

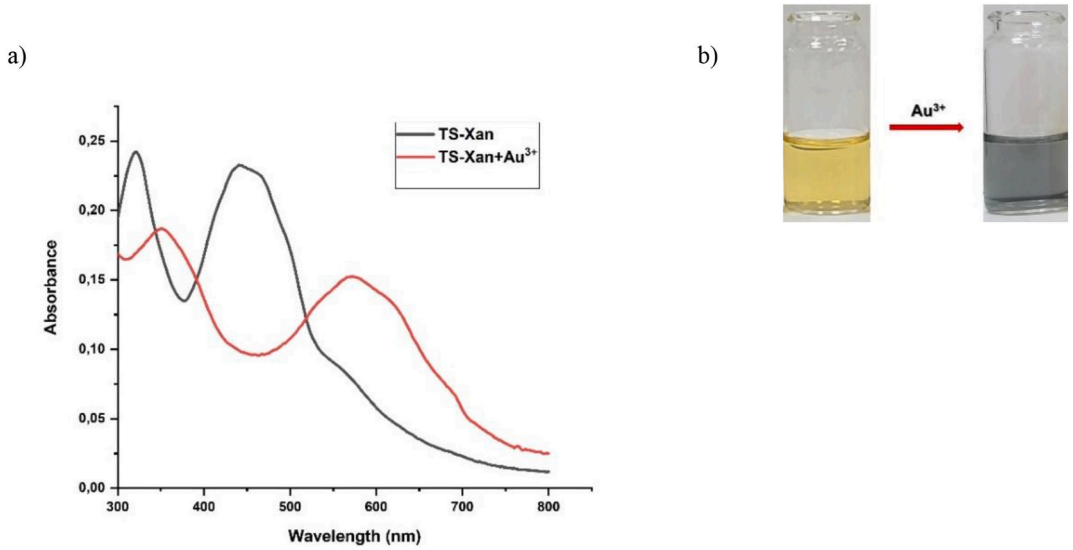

Fig. 2. a) Absorption spectra of **TS-Xan** (10 μM) and **TS-Xan + Au^{3+}** (1 eq Au^{3+}, 10 μM) in PBS (10 mM, pH = 7.4 at 25 °C) b) Chromogenic change of TS-Xan in PBS solution with the addition of 1 eq Au^{3+}.

the accompanying absorption shift serve as clear spectroscopic evidence of the interaction between TS-Xan and Au^{3+} ions, confirming the probe's effectiveness in Au^{3+} detection.

The selectivity of a colorimetric or fluorescent probe is one of its most critical attributes. To assess the selectivity of **TS-Xan** (10 μM in PBS, pH 7.4), its response to various metal ions, including Ag^{+}, Al^{3+}, Ba^{2+}, Ca^{2+}, Cd^{2+}, Co^{2+}, Cu^{2+}, Fe^{2+}, Fe^{3+}, Hg^{2+}, K^{+}, Li^{+}, Mg^{2+}, Mn^{2+}, Na^{+}, Ni^{2+}, Pb^{2+}, Pd^{3+}, and Zn^{2+}, was systematically investigated. In the selectivity experiment, **1 equivalent of Au^{3+}** and **10 equivalents** of other competing metal ions were introduced into the TS-Xan solution, and the resulting changes were monitored using UV–vis absorption spectroscopy. A distinct color change from yellow to violet was observed exclusively in the presence of Au^{3+} ions, whereas no noticeable color change occurred upon the addition of other metal ions, even at tenfold excess. Further UV–vis absorption analysis confirmed that upon Au^{3+} binding, the absorption peak at 441 nm disappeared, and a new peak emerged at 570 nm, indicating the formation of a TS-Xan–Au^{3+} complex. Notably, no significant spectral changes were detected despite the addition of 10 equivalents of other metal ions, as shown in Fig. 3. These results strongly demonstrate that TS-Xan exhibits an exceptionally high selectivity for Au^{3+} ions, making it a promising candidate for highly specific colorimetric detection in PBS solution.

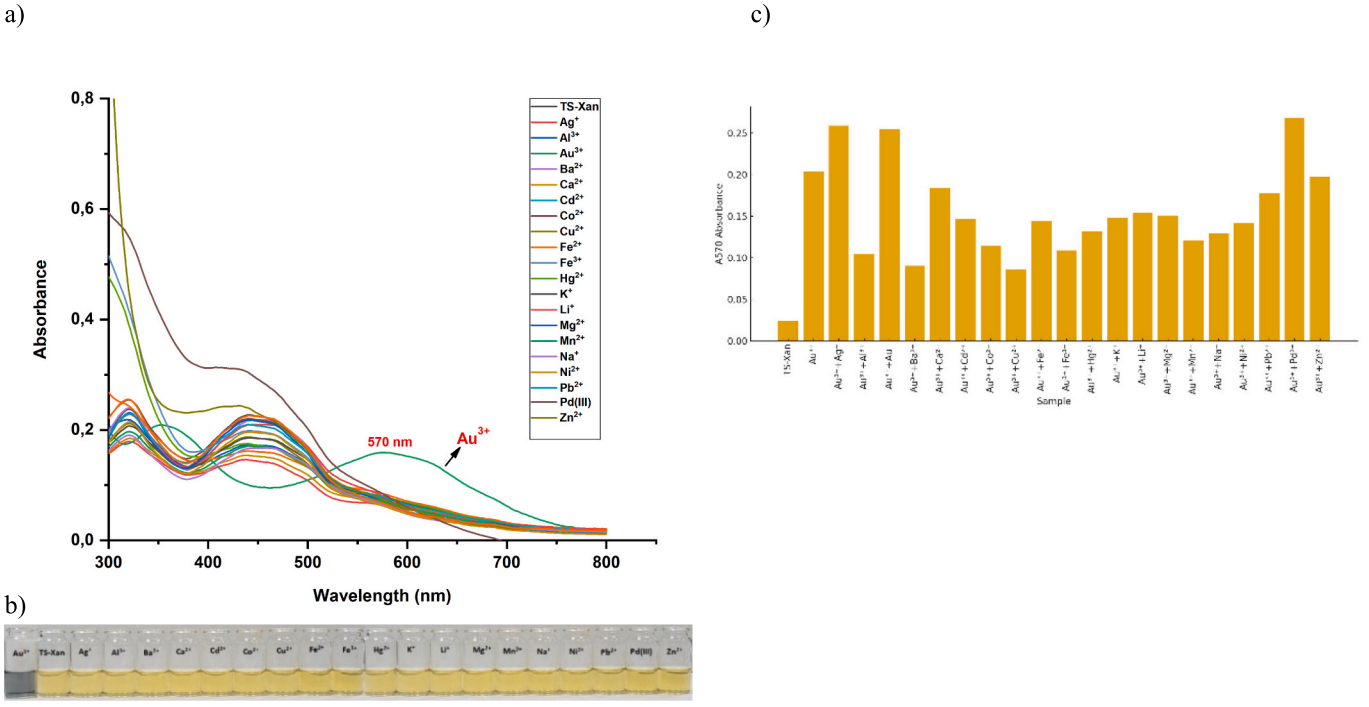

Fig. 3. a) Absorption spectra of **TS-Xan** (10 μM) in PBS (10 mM, pH = 7.4 at 25 °C) with the addition of **1 equivalent** Au^{3+} and **10 equivalents** of other metal ions: Ag^{+}, Al^{3+}, Ba^{2+}, Ca^{2+}, Cd^{2+}, Co^{2+}, Cu^{2+}, Fe^{2+}, Fe^{3+}, Hg^{2+}, K^{+}, Li^{+}, Mg^{2+}, Mn^{2+}, Na^{+}, Ni^{2+}, Pb^{2+}, Pd (III), Zn^{2+} b) Chromogenic change of **TS-Xan** in PBS solutions with the addition of metal ions: Ag^{+}, Al^{3+}, Ba^{2+}, Ca^{2+}, Cd^{2+}, Co^{2+}, Cu^{2+}, Fe^{2+}, Fe^{3+}, Hg^{2+}, K^{+}, Li^{+}, Mg^{2+}, Mn^{2+}, Na^{+}, Ni^{2+}, Pb^{2+}, Pd (III), Zn^{2+}. **c)** Bar graph displaying the absorbance values at 570 nm for mixtures containing TS-Xan, 1 equivalent of Au^{3+}, and 10 equivalents of each interfering metal ion.

The selectivity of TS-Xan toward Au^{3+} was confirmed by testing its response in the presence of 10-fold excess of various metal ions in PBS solution. Only Au^{3+} induced a distinct spectral and visual change, while other cations caused no significant interference. These findings demonstrate that TS-Xan maintains high selectivity for Au^{3+} even under competitive conditions, highlighting its potential for use in complex sample matrices.

The sensitivity of the TS-Xan probe (10 μM in PBS, pH 7.4) was systematically evaluated through a titration experiment, where the probe was exposed to increasing concentrations of Au^{3+} ions (0 to 10 equivalents) (Fig. 4). The spectral changes associated with different Au^{3+} concentrations were carefully analyzed to gain insights into the probe's detection capability. Upon the addition of 0.1 equivalent (1 μM) of Au^{3+}, a decrease in the absorption peak at 441 nm was observed, accompanied by the emergence of a new peak at 570 nm, indicating an interaction between Au^{3+} ions and TS-Xan. As the Au^{3+} concentration increased, these spectral changes became progressively more pronounced. For instance, with the addition of 0.4 equivalents of Au^{3+}, the absorption peak at 441 nm gradually diminished, while the 570 nm peak intensified. When the Au^{3+} concentration reached 0.6 equivalents (6 μM), the 441 nm peak completely disappeared, leaving only the characteristic TS-Xan–Au^{3+} complex absorption at 571 nm. At this stage, a visible color transition from yellow to violet was clearly noticeable. Upon further addition of 2 equivalents (20 μM) of Au^{3+}, the absorbance of the TS-Xan–Au^{3+} complex at 570 nm reached its maximum intensity. However, beyond this concentration, a gradual decrease in the 570 nm absorption peak was observed, likely due to excess Au^{3+} ions perturbing the complex equilibrium. These findings not only highlight the high sensitivity of TS-Xan toward Au^{3+} detection but also provide valuable insights into the interaction mechanism between the probe and Au^{3+} ions, further supporting its potential for quantitative colorimetric sensing applications.

Since reversibility is a crucial feature for practical sensor applications, the TS-Xan–Au^{3+} complex was treated with Na_2S (1:1) to evaluate the reversibility of the sensing mechanism. Upon the addition of 1 equivalent of Na_2S, a sharp decrease in the 570 nm absorption peak was observed, indicating the successful dissociation of the complex and partial restoration of the free probe. This reversibility can be explained by the strong affinity of sulfide ions (S^{2-}), introduced by Na_2S, toward Au^{3+} ions. Sulfide ions preferentially form a stable and insoluble gold sulfide complex (Au_2S_3), resulting in the displacement of Au^{3+} from the sensor and the regeneration of the free TS-Xan molecule. To further investigate the extent of reversibility, the complex solution was treated with varying equivalents of Na_2S, and the exact conversion efficiency was determined. When 5 equivalents of Na_2S were introduced, the 570 nm peak completely disappeared, while the original absorption peak of TS-Xan at 441 nm reappeared, confirming the full regeneration of the probe (Fig. 5). Moreover, this process was accompanied by a distinct visual transition from violet to yellow, demonstrating the rapid and complete reversibility of the sensor system upon Na_2S treatment. To assess the reusability of the system, the sensor was subjected to two complete Au^{3+} binding and release cycles using Na_2S. In both cycles, the UV–Vis spectra and visual color changes were fully restored, with no noticeable loss in signal intensity or performance. These results indicate that TS-Xan retains its sensing capability over at least two reversible cycles, supporting its practical applicability in repeatable detection settings.

The Jobs plot analysis was conducted to determine the binding stoichiometry between TS-Xan and Au^{3+} ions. The absorbance differences ($A-A_0$) at 570 nm were plotted against the mole fraction of Au^{3+}, yielding a distinct maximum at 0.33 mol fraction (Fig. 6). This result indicates the formation of a 2:1 binding stoichiometry for the **TS-Xan-Au^{3+}** complex, suggesting that two TS-Xan molecules coordinate with one Au^{3+} ions in solution. To further elucidate the sensing mechanism of the TS-Xan–Au^{3+} complex, high-resolution mass spectrometry (HRMS) analysis was performed (Supporting Information, Fig. S4). The HRMS data revealed that Au^{3+} ions, coordinated with a single chloride atom, interact with TS-Xan molecules in a 2:1 ratio, leading to the formation of the TS-Xan–Au^{3+} complex. The mass spectrum exhibited a peak at m/z = 980.50, which corresponds to the calculated value of m/z = 980.36 for $C_{46}H_{52}AuClN_8O_2$ [2TS-Xan + Au^{3+} + Cl], confirming the proposed complex formation. Based on these findings, we propose that the sensing mechanism of TS-Xan–Au^{3+} complex formation involves the coordination of Au^{3+} ions with both the pyridyl and imine nitrogen atoms of two TS-Xan molecules, as illustrated in Fig. 7.

(total concentration of 100 μM) at 570 nm.

The colorimetric response of TS-Xan toward Au^{3+} ions arises from a coordination-based mechanism. Au^{3+} binds selectively to the imine and pyridyl nitrogen atoms of TS-Xan, forming a 2:1 ligand–metal complex, as confirmed by Job's plot and HRMS analysis (m/z = 980.50). This interaction induces an intramolecular charge transfer (ICT), leading to a bathochromic shift in the UV–Vis spectrum—from 441 nm to 570 nm—and a visible color change from yellow to violet. The reversibility of this process, demonstrated by Na_2S treatment, further supports a dynamic, non-destructive coordination mechanism. DFT calculations corroborate these findings by revealing significant changes in the

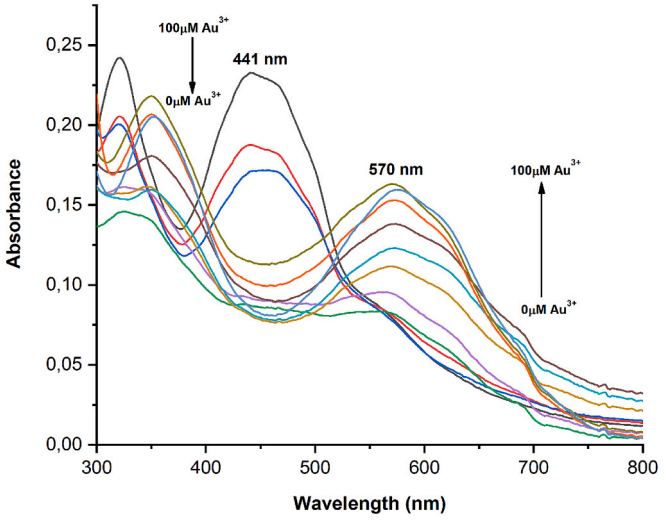

Fig. 4. Absorption spectra of **TS-Xan** (10 μM) in the presence of Au^{3+} (0–100 μM) in PBS (10 mM, pH = 7.4 at 25 °C).

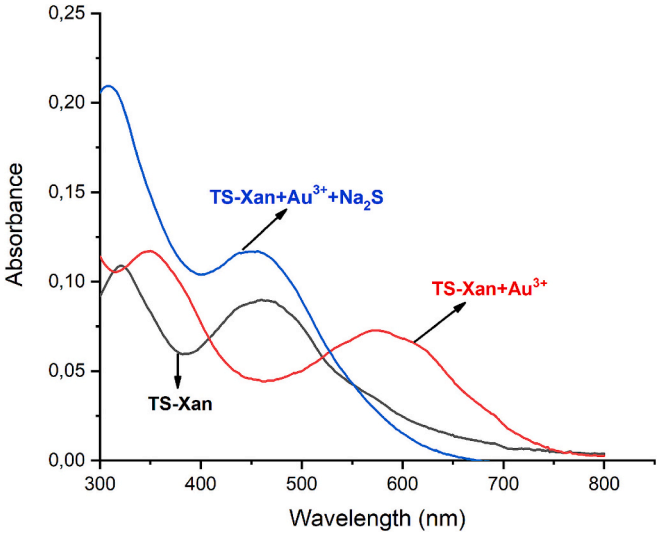

Fig. 5. Absorption spectra of TS-Xan prob. after adding Au^{3+} and Na_2S (reversibility experiment).

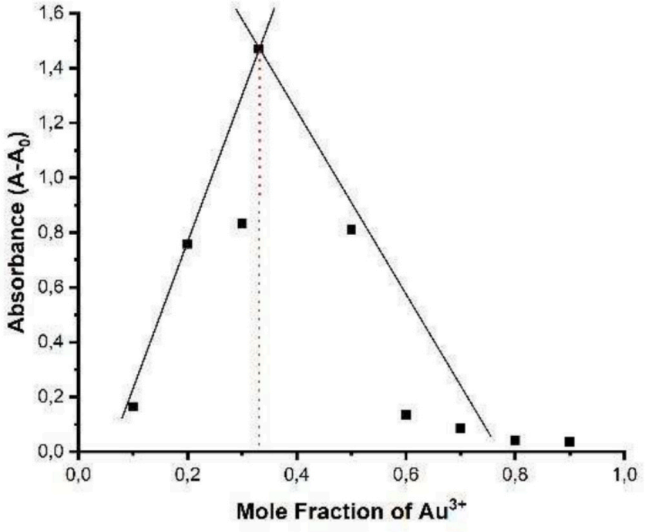

Fig. 6. Job's plot of **TS-Xan** and **Au^{3+}** in PBS (10 mM, pH = 7.4 at 25 °C).

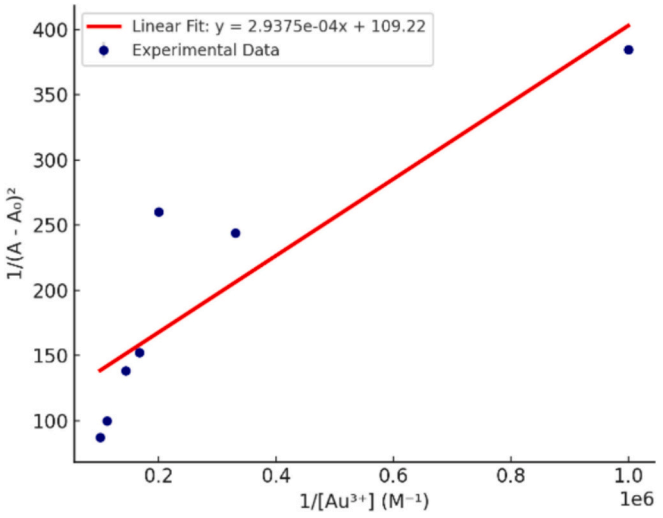

Fig. 8. Benesi-Hildebrand plot obtained from the absorption titration of TS-Xan with Au^{3+} in PBS (10 mM, pH = 7.4 at 25 °C).

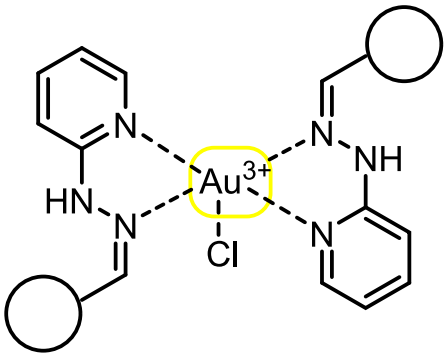

Fig. 7. Proposed mechanism for the detection of Au^{3+}.

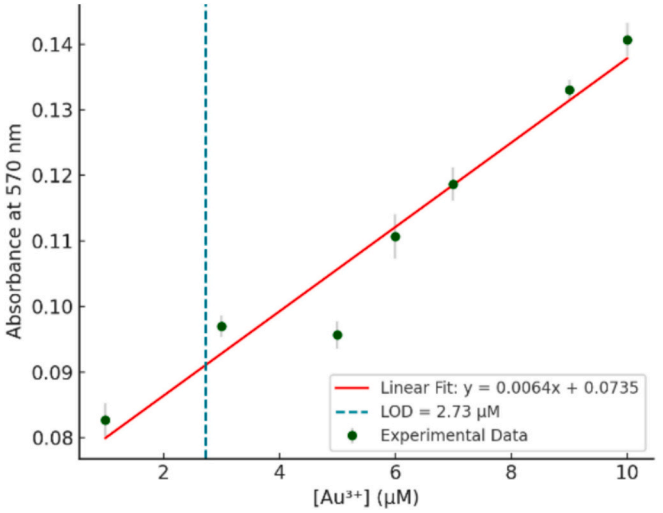

Fig. 9. Calibration curve for Au^{3+} detection & LOD.

electronic structure upon Au^{3+} binding.

The 2:1 binding stoichiometry between TS-Xan and Au^{3+} enhances the sensor's performance by providing a more stable and cooperative binding environment. Dual coordination increases the local density of chromophoric sites around the Au^{3+} ion, amplifying the colorimetric response through intramolecular charge transfer (ICT). This arrangement also improves complex stability in aqueous solution, contributing to the reproducibility and reversibility of the sensing process.

To evaluate the binding properties and sensitivity of the TS-Xan probe toward Au^{3+} ions, Benesi-Hildebrand analysis and limit of detection (LOD) calculations were performed. The Benesi- Hildebrand plot (Fig. 8) was constructed to determine the binding constant (K_α). The binding constant of TS-Xan toward Au^{3+} was calculated by using Benesi- Hildebrand equation for a 2:1 stoichiometric complex: $\frac{1}{(A-A_\circ)^2} = \frac{1}{K\alpha^2(A-A_\circ)^2[Au^{3+}]} + \frac{1}{(A-A_\circ)^2}$, where A and A_o are absorbances at 570 nm in the presence and absence of Au^{3+}. The calculation yielding a value of 3404.21 M^{-1}. This result supports a 2:1 (TS-Xan:Au^{3+}) binding model, indicating a strong interaction between the sensor and Au^{3+} ions. The high correlation of the linear regression suggests that the binding mechanism follows a well-defined complexation process, further validating the HRMS data.

The limit of detection (LOD) for Au^{3+} ions was determined using the 3σ/m method from the calibration curve (σ is the standart deviation of the blank solution and m is the slope) (Fig. 9). The resulting LOD value was 2.73 μM, indicating the sensor's high sensitivity and its ability to detect Au^{3+} at low concentrations. This detection limit is comparable to or lower than many previously reported colorimetric sensors. For instance, a coumarin-based probe reported by Wang et al. exhibited an LOD of 4.5 μM [40], while a rhodamine-based probe by Emrullahoglu et al. showed an LOD of approximately 3.6 μM [55]. In addition to its competitive sensitivity, TS-Xan offers advantages such as rapid response, reversibility, and ease of visual detection, making it a strong candidate for practical applications. The strong linear relationship observed in the calibration curve confirms the reliability and reproducibility of the probe's response. The combination of a well-defined binding constant and a low LOD value highlights the potential of TS-Xan as an efficient and selective colorimetric sensor for Au^{3+} detection in aqueous environments.

To further highlight the advantages of TS-Xan compared to other Au^{3+} probes, a comparative summary of recently reported sensors has been provided in Table S1 (Electronic Supplementary Information, ESI). Compared to previously developed probes, TS-Xan exhibits a rapid response time (<1 min), a distinct color change from yellow to violet visible to the naked eye, excellent selectivity toward Au^{3+} ions, and good reversibility. These features highlight the strong potential of TS-Xan for real-time and practical applications in environmental and analytical sensing.

To further assess the analytical performance of TS-Xan, a ratiometric evaluation was performed based on the absorbance ratio of the two distinct bands at 570 nm and 441 nm. Upon the gradual addition of Au^{3+} ions (0–10 μM), the absorbance at 570 nm increased while the original band at 441 nm decreased, indicating a concentration-dependent spectral shift. The resulting ratiometric plot (A_{570}/A_{441} vs. [Au^{3+}]) is presented in Fig. 10. Although the response was not strictly linear across the entire range, a pronounced and consistent trend was observed, particularly within the 0–1 μM range. This dual-band response mechanism confirms the ratiometric nature of TS-Xan, despite minor deviations at higher concentrations. This behavior, highlighted in the inset plot, supports the semi-quantitative detection capability of TS-Xan and reinforces its practical utility in trace-level Au^{3+} sensing applications.

In addition, to enhance the practicality of Au^{3+} detection, a paper-based strip test was developed by coating TS-Xan onto the surface of filter paper. The sensitivity of the TS-Xan-coated test strips was evaluated colorimetrically by treating them with different concentrations of Au^{3+} ions, ranging from 2×10^{-2} M to 1×10^{-4} M (Fig. 11). The results demonstrated that the TS-Xan-coated test strips enable rapid and highly sensitive Au^{3+} detection, making them a convenient tool for real-world applications. This method provides fast and accurate results without requiring complex instrumentation, offering a user-friendly, portable, and cost-effective approach for Au^{3+} detection in various chemical and environmental analyses.

While real environmental or biological samples were not tested in this study, the TS-Xan-coated paper strips demonstrated a distinct and rapid colorimetric response to Au^{3+} in PBS solution. These preliminary results suggest high potential for on-site applications, and future work will focus on validating performance in real sample matrices and comparing results with established analytical methods.

In the present study, the long-term stability of **TS-Xan-coated test strips** under different storage conditions was not systematically investigated. However, this is a highly relevant aspect for real-world application. While the TS-Xan sensor itself has shown excellent chemical stability when stored at 4 °C for over six months, future studies will include a detailed evaluation of the test strips' performance over time under various storage conditions such as ambient, refrigerated, and humid environments.

In addition to the experimental studies, the molecular structure and electronic properties of TS-Xan were investigated using density functional theory (DFT) calculations. For this purpose, the B3LYP functional [67,68] with the 6-31G(d) basis set [69] was used for the optimization of C, H, N, and O atoms, while the Au^{3+} ion was treated using the B3LYP/LANL2DZ functional and basis set [70–72]. Geometric optimizations and energy calculations were carried out using Gaussian 09 software [73], and the results were visualized with GaussView 5 [74]. These computational methods were selected to provide an accurate representation of the electronic structures and interactions within the system. The B3LYP functional and LANL2DZ basis set are widely utilized in the literature for the calculation of UV–Vis spectra of organic molecules and metal complexes [75]. Based on these calculations, the UV–Vis spectra of both free and Au^{3+}-bound TS-Xan molecules were thoroughly analyzed, and the correlation between spectroscopic properties and molecular structure was discussed.

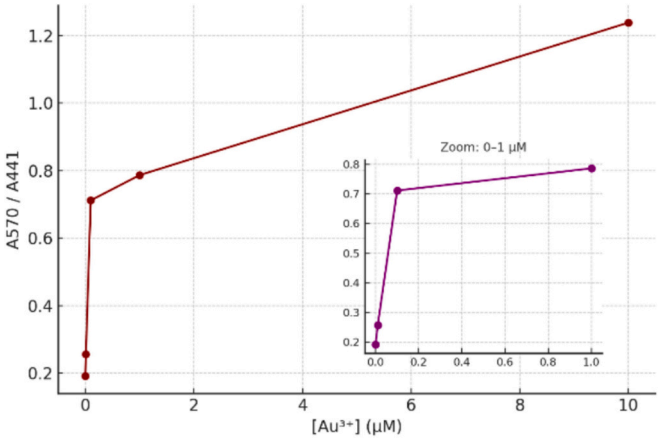

Fig. 10. Ratiometric absorbance response (A_{570}/A_{441}) of TS-Xan toward increasing concentrations of Au^{3+} ions (0–10 μM) in PBS (10 mM, pH 7.4). The main plot shows the full concentration range, while the inset highlights the ratiometric response within the 0–1 μM range, where a more consistent concentration-dependent trend is observed.

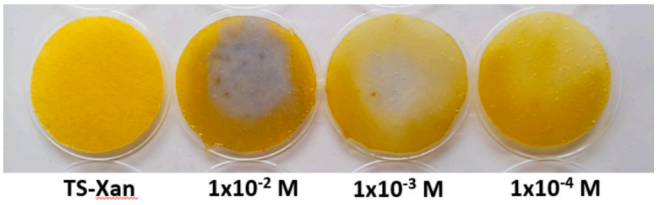

Fig. 11. Photographic representation of TS-Xan-coated test strips after exposure to varying concentrations of Au^{3+} ions.

Figs. 12(a) and (b) present the UV–Vis spectra of the two different molecular states of TS-Xan. In the free TS-Xan molecule, two distinct absorption peaks were observed: The first peak appears in the 200–400 nm range, with a maximum absorbance of 0.030. This region corresponds to the ultraviolet (UV) spectrum and is attributed to $\pi \rightarrow \pi^*$ or $n \rightarrow \pi^*$ electronic transitions. The strong absorption in this range indicates the high density of π bonds within the molecular structure and reflects the extent of conjugation in TS-Xan. The second peak is observed between 400 and 550 nm, with a maximum absorbance of 0.015. This range corresponds to the blue-green region of the visible light spectrum. The absorption of blue-green light results in the complementary color perception of the molecule, leading to its red-orange appearance.

In the UV–Vis spectrum of the TS-Xan + Au^{3+} complex, a single absorption peak was observed, located within the 400–1000 nm range, with a maximum absorbance of 0.004. The peak maximum appears around 600–700 nm, corresponding to the red-orange region of the visible spectrum. As a result, the complex absorbs light in this region, causing it to be perceived in its complementary color—blue-green tones. However, the low absorbance value (0.004) suggests that this color change is relatively faint and less intense. Additionally, the absence of a prominent peak in the UV region of the TS-Xan + Au^{3+} complex spectrum indicates that the electronic structure of the molecule has significantly changed upon complexation with the gold ion. This transition suggests that low-energy electronic transitions have become dominant, leading to a shift in the absorption properties of the complex.

The strong absorption peak observed in the UV region of the TS-Xan molecule suggests a high degree of conjugation and a π-electron dense structure. However, upon complexation with Au^{3+} ions, the disappearance of the UV absorption peak and the overall decrease in absorption intensity indicate that the gold ion significantly alters the electronic structure of the molecule. This interaction results in a modification of the energy levels associated with electronic transitions, leading to a shift in the optical properties of the system. Such effects of gold complexation on π-electron density and transition energies are well-documented in the literature [76], further supporting the observed spectral changes.

The UV absorption of TS-Xan highlights the role of conjugation in optical properties, while complexation with Au^{3+} ions leads to the disappearance of UV peaks and a weaker absorption in the visible region. This shift in optical behavior aligns with literature reports [77] on metal coordination effects and provides valuable insights for potential applications in dye chemistry and photochemical systems.

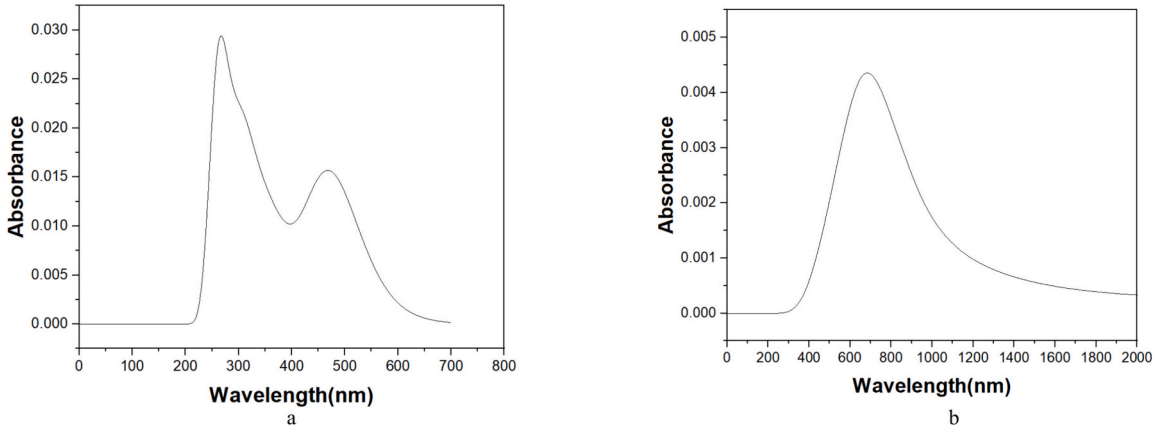

Fig. 12. Theoretical UV–Vis spectra of (a) TS-Xan and (b) TS-Xan-Au^{+3} complex.

4. Conclusion

In summary, a novel xanthene-based reversible colorimetric probe (TS-Xan) was successfully synthesized for the selective and sensitive detection of Au^{3+} ions. TS-Xan exhibited high selectivity toward Au^{3+} over various competing cations in PBS solution (10 mM, pH 7.4, 25 °C). The sensor displayed a unique UV–Vis absorption response at 570 nm, accompanied by a rapid colorimetric transition from yellow to violet within less than one minute, allowing for direct naked-eye detection. A key feature of TS-Xan is its reversible coordination mechanism with Au^{3+} ions. Upon the addition of Na_2S, the complexation is disrupted, and the sensor returns to its original state, resulting in a visual color shift from yellow to violet and back to yellow. This rapid, instrument-free detection capability offers significant advantages, making TS-Xan a highly practical tool for real-time monitoring of Au^{3+} ions. DFT calculations supported the experimental findings by confirming structural and electronic changes upon complexation with Au^{3+}. Notably, TS-Xan demonstrated a low limit of detection (2.73 μM), strong binding affinity ($K = 3404.21\ M^{-1}$), and exceptional selectivity over other metal ions, positioning it favorably among existing Au^{3+} sensors. Furthermore, its rapid, visible, and reversible response—combined with successful application in a paper-based test strip format—highlights its potential for real-time, cost-effective, and instrument-free detection in both laboratory and field settings. Taken together, these features establish TS-Xan as a highly practical and versatile platform for gold ion sensing. Future studies will aim to expand its scope toward other heavy metals and further enhance its analytical performance.

TS-Xan was specifically designed to target Au^{3+} ions through coordination with imine and pyridyl nitrogen atoms, which serve as strong binding sites for soft Lewis acid centers like gold(III). Given its modular structure, further chemical modifications may allow the extension of its sensing capabilities to other heavy metal ions or different oxidation states of gold. This adaptability offers promising opportunities for developing a broader family of TS-Xan-based colorimetric sensors

To improve the practical applicability of TS-Xan, future work will focus on integrating the sensor into portable platforms such as smartphone-assisted paper devices or microfluidic systems. Sensitivity enhancement through structural modification or signal amplification strategies is also planned, along with validation in real environmental and biological samples.

CRediT authorship contribution statement

Nuriye Tuna Subasi: Writing – original draft, Visualization, Methodology, Formal analysis, Data curation, Conceptualization.

Declaration of competing interest

The authors declare the following financial interests/personal relationships which may be considered as potential competing interests:

Nuriye Tuna Subasi reports equipment, drugs, or supplies was provided by Izmir Institute of Technology. If there are other authors, they declare that they have no known competing financial interests or personal relationships that could have appeared to influence the work reported in this paper.

Acknowledgements

I would like to express my sincere gratitude to Prof. Dr. Mustafa Emrullahoğlu for his invaluable support, expert guidance, and continuous encouragement throughout my studies. It has been an honor to work under his mentorship. I would also like to extend my heartfelt appreciation to Assoc. Prof. Tuncay Karakurt for his assistance and valuable contributions to the theoretical study This research did not receive any specific grant from funding agencies in the public, commercial, or not-for-profit sectors.

Appendix A. Supplementary data

Supplementary data to this article can be found online at https://doi.org/10.1016/j.sbsr.2025.100799.

Data availability

The data supporting this article have been included as part of the supplementary information

References

[1] L.E. van Vlerken, M.M. Amiji, Multi-functional polymeric nanoparticles for tumour-targeted drug delivery, Expert Opin. Drug Deliv. 3 (2) (2006) 205–216, https://doi.org/10.1517/17425247.3.2.205.
[2] E.C. Dreaden, A.M. Alkilany, X.H. Huang, C.J. Murphy, M.A. El-Sayed, The golden age: gold nanoparticles for biomedicine, Chem. Soc. Rev. 41 (2012) 2740–2779, https://doi.org/10.1039/C1CS15237H.
[3] M. Bouché, J.C. Hsu, Y.C. Dong, J. Kim, K. Taing, D.P. Cormode, Recent advances in molecular imaging with gold nanoparticles, Bioconjug. Chem. 31 (2) (2020) 303–314, https://doi.org/10.1021/acs.bioconjchem.9b00669.
[4] G.M. Sulaiman, H.M. Waheeb, M.S. Jabir, S.H. Khazaal, Y.H. Dewir, Y. Naidoo, Hesperidin loaded on gold nanoparticles as a drug delivery system for a successful biocompatible, anti-Cancer, anti-inflammatory and phagocytosis inducer model, Sci. Rep. 10 (2020) 9362, https://doi.org/10.1038/s41598-020-66419-6.
[5] A.S.K. Hash, Gold-catalyzed organic reactions, Chem. Rev. 107 (7) (2007) 3180–3211, https://doi.org/10.1021/cr000436x.
[6] A. Arcadi, Alternative synthetic methods through new developments in catalysis by gold, Chem. Rev. 108 (8) (2008) 3266–3325, https://doi.org/10.1021/cr068435d.
[7] Z. Li, C. Brouwer, C. He, Gold-catalyzed organic transformations, Chem. Rev. 108 (8) (2008) 3239–3265, https://doi.org/10.1021/cr068434l.

[8] N. Mariona, S.P. Nolan, N-heterocyclic carbenes in gold catalysis, Chem. Soc. Rev. 37 (2008) 1776–1782, https://doi.org/10.1039/B711132K.

[9] A. Corma, A. Leyva-Pérez, M.J. Sabater, Gold-catalyzed carbon−heteroatom bond-forming reactions, Chem. Rev. 111 (3) (2011) 1657–1712, https://doi.org/10.1021/cr100414u.

[10] M. Rudolph, A.S.K. Hashmi, Gold catalysis in total synthesis-an update, Chem. Soc. Rev. 41 (2012) 2448–2462, https://doi.org/10.1039/C1CS15279C.

[11] R. Dorel, A.M. Echavarren, Gold(I)-catalyzed activation of alkynes for the construction of molecular complexity, Chem. Rev. 115 (17) (2015) 9028–9072, https://doi.org/10.1021/cr500691k.

[12] L. Messori, G. Marcon, Gold complexes in the treatment of rheumatoid arthritis, Met. Ions Biol. Syst. 41 (2004) 279.

[13] I. Ott, On the medicinal chemistry of gold complexes as anticancer drugs, Coord. Chem. Rev. 253 (11−12) (2009) 1670–1681, https://doi.org/10.1016/j.ccr.2009.02.019.

[14] C.I. Yeo, K.K. Ooi, E.R.T. Tiekink, Gold-based medicine: a paradigm shift in anti-Cancer therapy? Molecules 23 (6) (2018) 1410, https://doi.org/10.3390/molecules23061410.

[15] S. Yue, M. Luo, H. Liu, S. Wei, Recent advances of gold compounds in anticancer immunity, Front. Chem. 8 (2020) 543, https://doi.org/10.3389/fchem.2020.00543.

[16] C.F. Shaw, Gold-based therapeutic agents, Chem. Rev. 99 (9) (1999) 2589–2600, https://doi.org/10.1021/cr980431o.

[17] M. Navarro, Gold complexes as potential anti-parasitic agents, Coord. Chem. Rev. 253 (2009) 1619–1626, https://doi.org/10.1016/j.ccr.2008.12.003.

[18] A. Habib, M. Tabata, Oxidative DNA damage induced by HEPES (2-[4-(2-hydroxyethyl)-1-piperazinyl]ethanesulfonic acid) buffer in the presence of au(III), J. Inorg. Biochem. 98 (11) (2004) 1696–1702, https://doi.org/10.1016/j.jinorgbio.2004.07.005.

[19] E. Nyarko, T. Hara, D.J. Grab, A. Habib, Y. Kim, O. Nikolskaia, T. Fukuma, M. Tabata, In vitro toxicity of palladium(II) and gold(III) porphyrins and their aqueous metal ion counterparts on *Trypanosoma brucei brucei* growth, Chem. Biol. Interact. 148 (2004) 19–25, https://doi.org/10.1016/j.cbi.2004.03.004.

[20] C.M. Goodman, C.D. McCusker, T. Yilmaz, V.M. Rotello, Toxicity of gold nanoparticles functionalized with cationic and anionic side chains, Bioconjug. Chem. 15 (4) (2004) 897–900, https://doi.org/10.1021/bc049951i.

[21] C.J. Fleming, E.L. Salisbury, P. Kirwan, D.M. Painter, R.S. Barnetson, Chrysiasis after low-dose gold and UV light exposure, J. Am. Acad. Dermatol. 34 (1996) 349–351, https://doi.org/10.1016/s0190-9622(07)80006-5.

[22] A.B.G. Lansdown, GOLD: human exposure and update on toxic risks, Crit. Rev. Toxicol. 48 (7) (2018) 596–614, https://doi.org/10.1080/10408444.2018.1513991.

[23] H.K. Fouad, R.M. Elrakaiby, M.D. Hashim, The application of flame atomic absorption spectrometry for gold determination in some of its bearing rocks, Am. J. Anal. Chem. 6 (2015) 411–421, https://doi.org/10.4236/ajac.2015.65040.

[24] D. Xue, H. Wang, Y. Liu, P. Shen, Multicolumn solid phase extraction with hybrid adsorbent and rapid determination of au, Pd and Pt in geological samples by GF-AAS, Min. Eng. 81 (2015) 149–151, https://doi.org/10.1016/j.mineng.2015.07.025.

[25] W. Guo, W. Xie, L. Jin, Q. Guo, S. Hu, Determination of sub-ng g^{-1} au in geological samples by ion molecule reaction ICP-MS and CH_4 plasma modifier, RSC Adv. 5 (2015) 103189–103194, https://doi.org/10.1039/C5RA19692B.

[26] X. Tang, B. Li, J. Lu, H. Liu, Y. Zhao, Gold determination in soil by ICP-MS: comparison of sample pretreatment methods, J. Anal. Sci. Technol. 11 (2020) 45, https://doi.org/10.1186/s40543-020-00245-3.

[27] H.B. Senturk, A. Gundogdu, V.N. Bulut, C. Duran, M. Soylak, L. Elci, M. Tufekci, Separation and enrichment of gold(III) from environmental samples prior to its flame atomic absorption spectrometric determination, J. Hazard. Mater. 149 (2007) 317–323, https://doi.org/10.1016/j.jhazmat.2007.03.083.

[28] C. Zeng, L. Tang, Determination of gold by flame atomic absorption spectrometry with hollow Fiber liquid phase microextraction using room temperature ionic liquids, Anal. Lett. 46 (2013) 1442–1453, https://doi.org/10.1080/00032719.2013.766799.

[29] A.C. Kasper, H.M. Veit, M. García-Gabaldón, V.P. Herranz, Electrochemical study of gold recovery from ammoniacal thiosulfate, simulating the PCBs leaching of mobile phones, Electrochim. Acta 259 (2018) 500–509, https://doi.org/10.1016/j.electacta.2017.10.161.

[30] Y. Wu, R.Y. Lai, Electrochemical gold(III) sensor with high sensitivity and tunable dynamic range, Anal. Chem. 88 (2016) 2227–2233, https://doi.org/10.1021/acs.analchem.5b03868.

[31] D.T. Quang, J.S. Kim, Fluoro- and chromogenic Chemodosimeters for heavy metal ion detection in solution and biospecimens, Chem. Rev. 110 (2010) 6280–6301, https://doi.org/10.1021/cr100154p.

[32] J.F. Zhang, Y. Zhou, J. Yoon, J.S. Kim, Recent progress in fluorescent and colorimetric chemosensors for detection of precious metal ions (silver, gold and platinum ions), Chem. Soc. Rev. 40 (2011) 3416–3429, https://doi.org/10.1039/C1CS15028F.

[33] S. Singha, D. Kim, H. Seo, S.W. Cho, K.H. Ahn, Fluorescence sensing systems for gold and silver species, Chem. Soc. Rev. 44 (2015) 4367–4399, https://doi.org/10.1039/C4CS00328D.

[34] M. She, Z. Wang, J. Chen, Q. Li, P. Liu, F. Chen, S. Zhang, J. Li, Design strategy and recent progress of fluorescent probe for noble metal ions (Ag, Au, Pd, and Pt), Coord. Chem. Rev. 432 (2021) 213712, https://doi.org/10.1016/j.ccr.2020.213712.

[35] D. Wu, A.C. Sedgwick, T. Gunnlaugsson, E.U. Akkaya, J. Yoon, T.D. James, Fluorescent chemosensors: the past, present and future, Chem. Soc. Rev. 46 (2017) 7105–7123, https://doi.org/10.1039/C7CS00240H.

[36] S.-H. Park, N. Kwon, J.-H. Lee, J. Yoon, I. Shin, Synthetic ratiometric fluorescent probes for detection of ions, Chem. Soc. Rev. 49 (2020) 143–179, https://doi.org/10.1039/C9CS00243J.

[37] S. Jantra, T. Palaga, P. Rashatasakhon, M. Sukwattanasinitt, S. Wacharasindhu, A "turn on" fluorometric and colorimetric probe based on vinylphenol-BODIPY for selective detection of au(III) ion in solution and in living cells, Dyes Pigments 191 (2021) 109341, https://doi.org/10.1016/j.dyepig.2021.109341.

[38] D. Plaisathit, K. Setthakarn, J. Sirirak, P. Swanglap, A. Kamkaew, P. Maitarad, K. Burgess, N. Wanichacheva, Novel near-infrared Aza-BODIPY-based fluorescent and colorimetric sensor for highly selective detection of Au^{3+} in aqueous media, human skin and brain cells, J. Photochem. Photobiol. A Chem. 441 (2023) 114713, https://doi.org/10.1016/j.jphotochem.2023.114713.

[39] K. Naksomboon, N. Kaewchangwat, W. Sirisaksoontorn, K. Suttisintong, A novel indolino-spironaphthooxazine as the highly sensitive and selective probe for colorimetric detection of Au^{3+}, Dyes Pigments 214 (2023) 111193 https://doi.org/10.1016/j.dyepig.2023.111193.

[40] Q. Wang, Y. Feng, J. Jiang, W.-J. Wang, J.-Y. Chen, H.-T. Sheng, X.-M. Meng, M.-Z. Zhu, A coumarin-based colorimetric and fluorescent probe for the highly selective detection of Au^{3+} ions, Chin. Chem. Lett. 27 (9) (2016) 1563–1566, https://doi.org/10.1016/j.cclet.2016.02.021.

[41] G. Suna, E. Erdemir, L. Liv, S. Gunduz, T. Ozturk, E. Karakuş, Multi-channel detection of au(III) ions by a novel rhodamine based probe, Sensors Actuators B Chem. 360 (2022) 131658, https://doi.org/10.1016/j.snb.2022.131658.

[42] K. Yang, L. Pan, L. Gong, Q. Liu, Z. Li, L. Wu, Y. He, Colorimetric and visual determination of au(III) ions using PEGylated gold nanoparticles, Microchim. Acta 185 (2018) 95, https://doi.org/10.1007/s00604-017-2648-7.

[43] H. Seo, M.E. Jun, O.A. Egorova, K.-H. Lee, K.-T. Kim, K.H. Ahn, A reaction-based sensing scheme for gold species: introduction of a (2-Ethynyl)benzoate reactive moiety, Org. Lett. 14 (19) (2012) 5062–5065, https://doi.org/10.1021/ol302291c.

[44] N.T. Patil, V.S. Shinde, M.S. Thakare, P.H. Kumar, P.R. Bangal, A.K. Barui, C. R. Patra, Exploiting the higher alkynophilicity of au-species: development of a highly selective fluorescent probe for gold ions, Chem. Commun. 48 (2012) 11229–11231, https://doi.org/10.1039/C2CC35083A.

[45] S. Kambam, B. Wang, F. Wang, Y. Wang, H. Chen, J. Yin, X. Chen, A highly sensitive and selective fluorescein-based fluorescence probe for Au^{3+} and its application in living cell imaging, Sensors Actuators B Chem. 209 (2015) 1005–1010, https://doi.org/10.1016/j.snb.2014.12.085.

[46] C. Çetintas, E. Karakus, M. Üçüncü, M. Emrullahoglu, A fluorescein-based chemodosimeter for selective gold(III) ion monitoring in aqueous media and living systems, Sensors Actuators B Chem. 234 (2016) 109–114, https://doi.org/10.1016/j.snb.2016.04.158.

[47] M. Üçüncü, E. Karakus, M. Emrullahoglu, A BODIPY/pyridine conjugate for reversible fluorescence detection of gold(III) ions, New J. Chem. 39 (2015) 8337–8341, https://doi.org/10.1039/C5NJ01664A.

[48] M. Üçüncü, E. Karakus, M. Emrullahoglu, A BODIPY-based fluorescent probe for ratiometric detection of gold ions: utilization of Z-enynol as the reactive unit, Chem. Commun. 52 (2016) 8247–8250, https://doi.org/10.1039/C6CC04100K.

[49] J.-B. Wang, Q.-Q. Wu, Y.-Z. Min, Y.-Z. Liu, Q.-H. Song, A novel fluorescent probe for au(III)/au(I) ions based on an intramolecular hydroamination of a Bodipy derivative and its application to bioimaging, Chem. Commun. 48 (2012) 744–746, https://doi.org/10.1039/C1CC16128H.

[50] Y. Wang, Y. Liu, J. Miao, M. Ren, W. Guo, X. Lv, A novel Bodipy-based fluorescent probe for Au^{3+} ions with high selectivity and its application to bioimaging, Sensors Actuators B Chem. 226 (2016) 364–369, https://doi.org/10.1016/j.snb.2015.12.009.

[51] C. Cantürk, M. Üçüncü, M. Emrullahoglu, A BODIPY-based fluorescent probe for the differential recognition of Hg(II) and Au(III) ions, RSC Adv. 5 (2015) 30522–30525, https://doi.org/10.1039/C5RA04015A.

[52] B. Wang, T. Fu, S. Yang, J. Li, Y. Chen, An intramolecular charge transfer (ICT)-based dual emission fluorescent probe for the ratiometric detection of gold ions, Anal. Methods 5 (2013) 3639–3641, https://doi.org/10.1039/C3AY40450A.

[53] J.H. Do, H.N. Kim, J. Yoon, J.S. Kim, H.-J. Kim, A rationally designed fluorescence turn-on probe for the gold(III) ion, Org. Lett. 12 (5) (2010) 932–934, https://doi.org/10.1021/ol902860f.

[54] O.A. Egorova, H. Seo, A. Chatterjee, K.H. Ahn, Reaction-based fluorescent sensing of au(I)/au(III) species: mechanistic implications on Vinylgold intermediates, Org. Lett. 12 (3) (2010) 401–403, https://doi.org/10.1021/ol902395x.

[55] M. Emrullahoglu, E. Karakus, M. Üçüncü, A rhodamine based "turn-on" chemodosimeter for monitoring gold ions in synthetic samples and living cells, Analyst 138 (2013) 3638–3641, https://doi.org/10.1039/C3AN00024A.

[56] F. Song, H. Ning, H. She, J. Wang, X. Peng, A turn-on fluorescent probe for Au^{3+} based on rodamine derivative and its bioimaging application, Sci. China Chem. 57 (2014) 1043–1047, https://doi.org/10.1007/s11426-014-5107-x.

[57] P. Srisuratsiri, P. Kanjanasirirat, A. Chairongdua, P. Kongsaeree, Reversible rhodamine-alkyne Au^{3+}-selective chemosensor and its bioimaging application, Tetrahedron Lett. 58 (2017) 3194–3199, https://doi.org/10.1016/j.tetlet.2017.07.014.

[58] J.Y. Choi, G.-H. Kim, Z. Guo, H.Y. Lee, K.M.K. Swamy, J. Pai, S. Shin, I. Shin, J. Yoon, Highly selective ratiometric fluorescent probe for Au^{3+} and its application to bioimaging, Biosens. Bioelectron. 49 (2013) 438–441, https://doi.org/10.1016/j.bios.2013.05.033.

[59] M. Dong, Y.-W. Wang, Y. Peng, Highly selective ratiometric fluorescent sensing for Hg^{2+} and Au^{3+}, respectively, in aqueous media, Org. Lett. 12 (22) (2010) 5310–5313, https://doi.org/10.1021/ol1024585.
[60] S. Adhikari, S. Mandal, A. Ghosh, P. Das, D. Das, Strategically modified rhodamine–quinoline conjugate as a CHEF-assisted FRET probe for Au^{3+}: DFT and living cell imaging studies, J. Organomet. Chem. 80 (17) (2015) 8530–8538, https://doi.org/10.1021/acs.joc.5b01141.
[61] H.K. Mackenzie, B.W. Rawe, K. Samedov, H.T.G. Walsgrove, A. Uva, Z. Han, D. P. Gates, A smart phosphine–diyne polymer displays "turn-on" emission with a high selectivity for gold(I/III) ions, J. Am. Chem. Soc. 142 (23) (2020) 10319–10324, https://doi.org/10.1021/jacs.0c04330.
[62] Y.R. Bhorge, T.-L. Chou, Y.-Z. Chen, Y.-P. Yen, New coumarin-based dual chromogenic probe: naked eye detection of copper and silver ions, Sensors Actuators B Chem. 220 (2015) 1139–1144, https://doi.org/10.1016/j.snb.2015.06.059.
[63] D. Divya, S. Thennarasu, A novel isatin-based probe for ratiometric and selective detection of Hg^{2+} and Cu^{2+} ions present in aqueous and environmental samples, Spectrochim. Acta A Mol. Biomol. Spectrosc. 243 (2020) 118796, https://doi.org/10.1016/j.saa.2020.118796.
[64] J. Benford-Ward, S. Ahmadipour, A. Sembayeva, L. Male, R.S. Grainger, Studies towards the synthesis of (+)-Dictyoxetane, Chem. Eur. J. 28 (71) (2022), https://doi.org/10.1002/chem.20220242.
[65] J. Chen, Y. Fang, L. Sun, F. Zeng, S. Wu, An activatable probe for detecting alcoholic liver injury via multispectral optoacoustic tomography and fluorescence imaging, Chem. Commun. 56 (2020) 11102–11105, https://doi.org/10.1039/D0CC04635C.
[66] M. Üçüncü, M. Emrullahoglu, A BODIPY-based reactive probe for the detection of au(III) species and its application to cell imaging, Chem. Commun. 50 (2014) 5884–5886, https://doi.org/10.1039/C4CC01958J.
[67] A.D. Becke, Density–functional thermochemistry. III. The role of exact exchange, J. Chem. Phys. 98 (1993) 5648–5652.
[68] C. Lee, W. Yang, R.G. Parr, Development of the Colle–Salvetti correlation–energy formula into a functional of the electron density, Phys. Rev. B 37 (1988) 785.
[69] J.B. Foresman, A. Frisch, Exploring Chemistry with Electronic Structure Methods: A Guide to Using Gaussian, 1996.
[70] P.J. Hay, W.R. Wadt, Ab initio effective core potentials for molecular calculations. Potentials for the transition metal atoms Sc to Hg, J. Chem. Phys. 82 (1985) 270–283.
[71] P.J. Hay, W.R. Wadt, Ab initio effective core potentials for molecular calculations. Potentials for K to Au including the outermost core orbitals, J. Chem. Phys. 82 (1985) 299–310.
[72] P.J. Hay, W.R. Wadt, Ab initio effective core potentials for molecular calculations. Potentials for main group elements Na to bi, J. Chem. Phys. 82 (1985) 284–298.
[73] M. Frisch, G. Trucks, H.B. Schlegel, G. Scuseria, M. Robb, J. Cheeseman, G. Scalmani, V. Barone, B. Mennucci, G. Petersson, Gaussian 09, Revision a. 02, Gaussian, Inc, Wallingford, CT, 2009.
[74] Gaussian, Inc (Ed.), GaussView, Version 5.0.9, Gaussian, Inc, Wallingford, CT, US, 2015.
[75] M.R. Taghartapeh, N.N. Pesyan, H. Rashidnejad, H.R. Khavasi, A. Soltani, Synthesis, spectroscopic and photophysical studies of xanthene derivatives, J. Mol. Struct. 1149 (2017) 862–873.
[76] J.J. Mihaly, S.M. Wolf, J.E. Haley, K. De La Harpe, T.A. Grusenmeyer, T.G. Gray, Nonlinear optical properties of molecular gold complexes, in: 2023 IEEE Research and Applications of Photonics in Defense Conference (RAPID), IEEE, 2023, pp. 1–2.
[77] R. Tandiana, N.T. Van-Oanh, C. Clavaguéra, Interaction between organic molecules and a gold nanoparticle: a quantum chemical topological analysis, Theor. Chem. Accounts 140 (8) (2021) 118.